SAND2015-7572J

Microstructural Evolution and Friction in Metals

N. Argibay[1], S. Cheng[2], W.G. Sawyer[3], J.R. Michael[1], M. Chandross[1]

[1] *Materials Science and Engineering Center, Sandia National Laboratories, Albuquerque, NM*
[2] *Department of Physics/Macromolecules and Interfaces Institute, Virginia Polytechnic Institute and State University, Blacksburg, VA*
[3] *Department of Mechanical and Aerospace Engineering, U. of Florida, Gainesville, FL*

Abstract

The prediction of macro-scale friction and wear behavior based on first principles and material properties has remained an elusive but highly desirable target for tribologists and material scientists alike. Stochastic processes (e.g. wear), statistically described parameters (e.g. surface topography) and their evolution tend to defeat attempts to establish practical general correlations between fundamental nanoscale processes and macro-scale behaviors. We present a model based on microstructural stability and evolution for the prediction of metal friction regimes, founded on recently established microstructural deformation mechanisms of nanocrystalline metals, that relies exclusively on material properties and contact stress models. We show through complementary experimental and simulation results that this model overcomes longstanding practical challenges and successfully makes accurate and consistent predictions of friction transitions for a wide range of contact conditions. This framework not only challenges the assumptions of conventional causal relationships between hardness and friction, and between friction and wear, but also suggests a pathway for the design of higher performance metal alloys.

Introduction

At sufficiently low applied stresses and temperatures it is possible for unlubricated or boundary lubricated pure, soft metal surfaces to evolve into remarkably low friction and low wear behavior associated with the formation and persistence of a stable ultra-nanocrystalline (UNC) surface film (*1*–*3*) with grain sizes well below 100 nm. It has been suggested (*2*) that this behavior of metal contacts relies on the transition from dislocation to grain boundary dominated plasticity at sufficiently small grain size (*4*–*6*). However, largely due to the highly stochastic and transient nature of tribological interfaces, the dominant mechanisms and bounding applied stress conditions wherein this desirable behavior can be achieved have eluded clear definition (*7*, *8*). We propose a microstructural stability framework that can accurately predict the time, temperature and stress-dependent conditions where this phenomenon occurs, and correlate these regimes of measured tribological response to the specifics of the evolving surface microstructure.

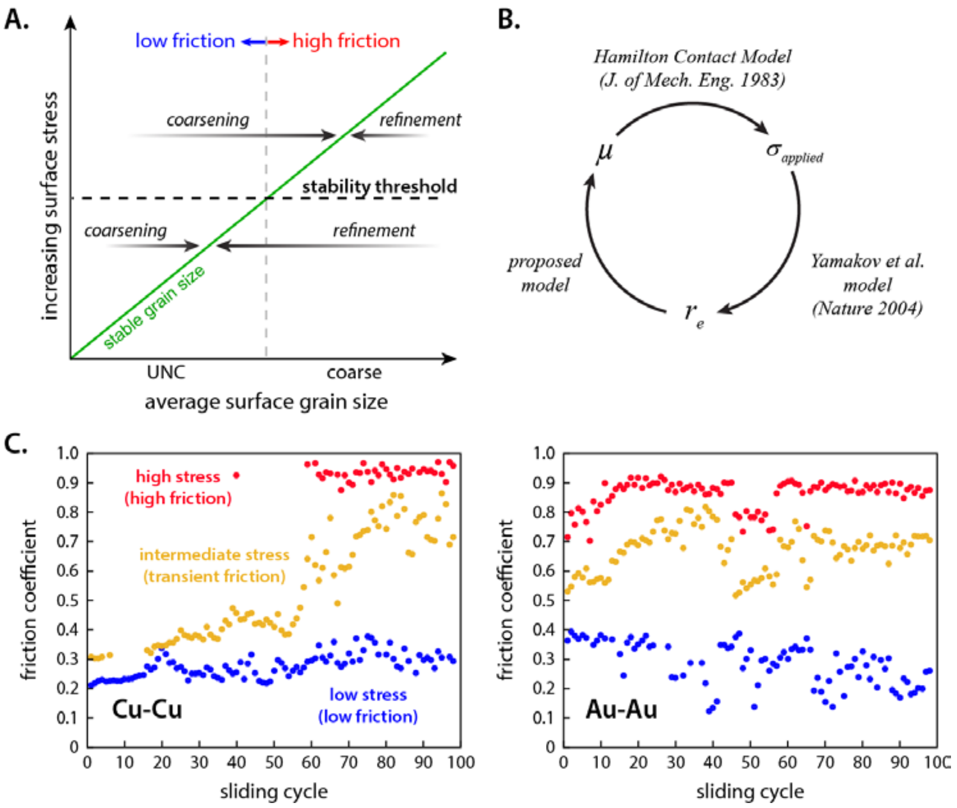

Fig. 1. *(A) Schematic of friction regimes as a function of surface grain size and surface stress, (B) a diagram of the framework that defines the stress-dependent microstructural evolution regimes, and (C) experimental results for sphere-on-flat friction experiments for Au-Au (in air) and Cu-Cu (in* N_2*) contacts where friction data was binned into three stress regimes highlighting the presence of stress thresholds that define whether friction coefficient will be perpetually low, high, or progressively increase (transient).*

Mechanistic Origin of Low Friction with Metals

We present evidence from molecular dynamics (MD) simulations demonstrating that grain boundary mediated plasticity (GBMP) is the source of low friction behavior, and that a transition to dislocation mediated plasticity (DMP) and high friction, occurs when sufficiently high surface stresses drive grain coarsening (see Fig. 1). While wear can effectively reset the surface microstructure, recovering low friction for a short amount of time, it does not generally occur on a faster timescale than microstructure coarsening for pure metals. We propose a quantitative friction-regime model for metals that is based on established literature detailing the stress-dependent deformation mechanisms of nanocrystalline metals(*6*, *9*, *10*). We show that this mechanistic framework explains the correlation between hardness and low friction by linking these macroscale properties to atomistic processes. Our proposed model provides quantitative expressions predicting the stress and time dependent boundaries of (1) a regime where UNC surface films and low friction are stable over long times, (2) a regime of quasi or transient stability and (3) a regime where low friction surface films are unachievable.

The model is based on the postulate from Yamakov, *et al.*(*6*) that the grain size in a metal under stress is driven towards the equilibrium dislocation splitting distance, r_e. We propose that this is an integral part of a feedback loop in which surface stress dictates the size of grains at the surface, which then implies the dominant sliding mechanism (DMP or GBMP), and thus the friction coefficient. The friction coefficient then feeds back into the magnitude of the surface stress through Hamilton's contact model(*11*, *12*). At low surface stresses, this feedback loop ensures small grains and low friction (with coefficient, $\mu \sim 0.3$), whereas at high stresses positive feedback implies that coarsening dominates grain refinement (e.g. cold-working of the surface), and friction will be high ($\mu >\sim 0.7$).

Greenwood and Williamson (*13*) and Archard (*14*) showed that contact models for ideally smooth curved surfaces may be used to describe stress distributions in the vicinity of the contact, even when the real contact area differs significantly from the apparent area of contact and consists of multiple, smaller elasto-plastic asperity contacts (*15*). In the regime of low average surface stress, microscopic contacts lead to local plastic deformation which rapidly evolves grain sizes towards the low stress limit. This limiting nanocrystalline (NC) grain size is expected for such nanoscopic contact events, and has been observed in a number of experiments (*1*, *2*, *16*). Following Yamakov *et al.*(*6*), the dominant mechanism for deformation of NC systems below the yield strength is GBMP. Nanocrystalline surfaces have a large density of grain boundaries that not only promote low friction across the sliding interfaces but also low wear as material is easily transferred between mating surfaces and not immediately shed from the contact. With low surface stress the friction coefficient associated with GBMP is remarkably low. Thus, there exists a stable, low friction and wear regime for metal contacts with an origin in the generation of NC surface layers that allow for easy shearing and deformation along grain boundaries.

We show that a stable low friction regime only exists at a surface stress less than half of the theoretical strength of the material (σ_∞). For stresses above this threshold, the opportunity for the formation of stable NC grains is reduced. With increased surface stress, deformation begins to be accommodated by full and partial dislocations, with a significant penalty in energy dissipation. The result is a loss of stability and a transition to DMP, leading to larger grained material with higher friction coefficients and wear rates. At stresses above σ_∞, DMP is always the prevailing deformation mechanism, and low friction is never observed.

MD Simulations and a Microstructural Evolution Model of Metal Friction

We have performed large-scale molecular dynamics (MD) simulations of shear in pure metals (Ag and Au) and alloys (Ag-Cu) in order to resolve the fundamental tribological mechanisms responsible for high friction in the former and low friction in the latter. Nanocrystalline Ag and Au substrates were created with a melt/quench procedure, followed by a random replacement of 12.5% of the atoms to create the alloy structures. Shear simulations proceeded with either a hemispherical slider (10 nm radius), or mobile or rigid slabs, as appropriate.

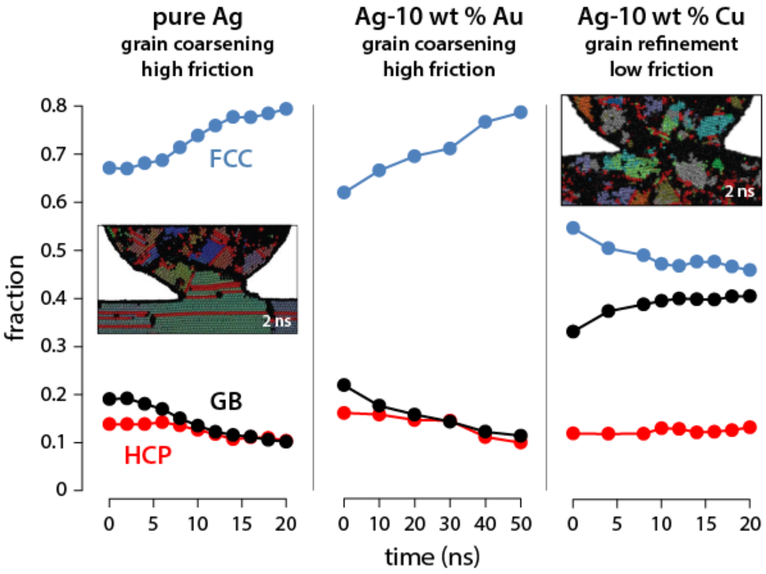

Fig. 2. *Evolution in grain boundary density for slabs of (left) pure, (middle) soluble alloy and (right) insoluble alloy after sliding at 300 MPa normal stress. Grain growth was found to occur in the pure and soluble alloy contacts, but the two-phase alloy contact exhibited grain refinement (GB stability) and deformation was primarily accommodated via GB sliding; tip radius was approximately 10 nm, and the two insets are representative snapshots after 2 ns of sliding.*

These simulations demonstrated that in both the pure metals and the alloys there was substantial cold welding at the contact point. The pure metals also showed grain reorientation and/or coarsening at the contact, leading to shear accommodation along the crystallographic slip planes (i.e. DMP) and relatively high friction (friction coefficient μ ≅ 0.2). The friction coefficients here are not to be numerically compared to the values from experiments, as these are nanoscale, single asperity simulations which are more comparable to friction force microscopy with an AFM. In the multi-phase alloy (with a known miscibility gap) there was no such reorientation, and shear was accommodated along the newly created grain boundary at the contact, with lower friction than the pure metals (μ ≅ 0.02). Calculations of the total number of FCC and grain boundary atoms during sliding contact showed that the pure metal underwent significant coarsening, while the alloy demonstrated some amount of grain refinement. These results demonstrate that the mechanism leading to low friction in alloys is identical to that causing Hall-Petch (HP) strengthening. Whereas in HP strengthening, grains that are smaller than ~100 nm show higher hardness because of their inability to support multiple dislocations, in these simulations it is instead the accessible slip systems that changes the friction coefficient. These are essentially the same mechanisms discussed by Yamakov *et al.*(*6*) In pure metals, coarsening leads to larger grains, and although MD cannot in general access grains above 100 nm, multiple dislocations can still be generated and the system shears along the crystallographic slip planes. In contrast, grain boundaries are stabilized in multi-phase alloys, and shear must be accommodated by GBMP.

In order to demonstrate that these two mechanisms are responsible for the differing frictional response, we designed targeted simulations in which both pure metals and multi-phase alloys are forced to shear with the same mechanisms (i.e. DMP or GBMP), and demonstrate that this leads to identical friction coefficients. To investigate DMP in the alloy, we slightly modify our system from the immiscible Ag-Cu alloy to a fully miscible Ag-Au alloy. Because Ag and Au have nearly the same lattice constant and atomic radius, we find that grain boundaries are no longer stabilized (as in Ag-Cu), and there is significant coarsening under shear. The calculated friction coefficient for the Ag-Au alloy is nearly identical to those for both pure Ag and pure Au ($\mu \sim 0.2$). To demonstrate lower friction with GBMP, we change the geometry of the simulations to preclude the coarsening mechanism that allows for DMP. To this end we use an infinite, rigid NC plate as a slider. While cold welding occurs and a contact film forms with this slider, its NC nature makes coarsening (leading to DMP) nearly impossible, and GBMP occurs in both the pure metal and the alloy, leading to low friction coefficients ($\mu \sim 0.02$).

In metallic contacts under shear, the microstructure at the contact is affected by a competition between grain refinement from cold-working and coarsening due to stress-assisted grain growth. The simulations show that these mechanisms are directly tied to the tribological response. When the applied stress is low refinement dominates, leading to GBMP and low friction. At higher applied stresses coarsening dominates and crystallographic slip is activated, leading to higher friction. Kinetic stabilization of GBs through Zener pinning or solute drag influences this competition by preventing or greatly reducing grain growth rates. Grain refinement is then enhanced, leading to the UNC layers seen in many low friction metal contacts (*1*, *2*, *16*, *17*).

These results indicate that the tribological response in metals is primarily driven by microstructure, and may be coalesced into a single, general model. The independent driving forces to be considered are applied stress, number of sliding cycles, and temperature, and for this initial study we will consider the first two only at room temperature (See Fig. 1A).

As a function of stress, it is instructive to start with the two extremes. At sufficiently high applied stresses the tribological response is dominated by plowing and gross abrasive wear as the slider is partially embedded in the substrate. The friction coefficient and wear rate in this regime will be high regardless of the number of sliding cycles, and the microstructure itself plays little role. We refer to this limit as the Tabor limit, where the applied mean stress of an axisymmetric elasto-plastic contact of arbitrary shape exceeds three times the flow stress in simple compression(*18*) (pp. 176-177). This relationship depends on hardness, and thus grain size and its evolution, but serves as an intrinsic limit of validity for the proposed model. This is an important concept, as we will show below that in high stacking fault energy (SFE) materials such as pure Al or Ni [see supplemental section S3] our predicted microstructural stability limits (explained below) may exist at surface stresses far higher than the Tabor limit. This implies that plowing will occur at stresses lower than those where we predict transitions in tribological behavior from evolution of the surface microstructure.

The Tabor limit is simply defined by the hardness of the material, which is itself a function of grain size, though to a significantly greater depth than the thickness of low friction UNC films; when applied stress exceeds the hardness the slider indents the substrate beyond the elastic limit and plowing occurs. The stability thresholds associated with surface grain size evolution require a more subtle argument. In the ensuing description a number of simplifications and assumptions of generality were required to arrive at a set of reduced (i.e. dimensionless) parameters that predict the stability bounds (i.e. reduced stress, $\tilde{\sigma}$, time, $\tilde{\tau}$, and temperature, $\tilde{\mathrm{T}}$). It is *post facto* apparent that these assumptions and simplifications are justified given the remarkable agreement with experimental evidence presented in Fig. 1B. We build on the work of Yamakov et al.(*6*) and others(*19–21*) and propose that these predicted microstructural stability limits can be described as a function of materials properties only.

At lower stresses, well below the Tabor limit for most pure FCC metals, grain refinement via sliding dominates and there is a stable regime of low friction due to GBMP (regime I). At moderate stresses a regime of quasi-stability is found. In this regime, at low integrated contact time (i.e. cycles) the initial microstructure -- assuming an initially NC structure -- dominates, leading to GBMP and low friction and wear (regime II). However, this response is transient, as at these intermediate stresses SAGG dominates over grain refinement and friction eventually transitions to higher values as the microstructure coarsens, and DMP takes over (boundary of II_A/II_B). Finally, at stresses above the theoretical yield strength of the material DMP is immediately active and the friction is always high (regime III).

These results are shown in Fig. 3A in the form of phase space maps, where we map out friction regimes as a function of reduced stress and reduced time. In regime I, surface grain boundaries are stable, grain refinement dominates, and friction is consistently low ($\mu < 0.4$). The upper limit for regime I is referred to as the Beilby limit based on early work on mechanical polishing (*22*) identifying the formation of a near-amorphous surface layer in boundary lubricated metal contacts. At stresses just above this lower stability threshold we find a quasi-stable regime where low friction transitions to higher friction ($0.4 < \mu < 0.7$), a process that is periodically restarted via wear. At yet higher stress (but generally below the Tabor limit) lies regime III where perpetually high friction is observed ($\mu > 0.8$), even without plowing or cutting. As this upper stability limit is expected to correspond to stresses approaching the theoretical strength of a NC metal it is referred to as the Hall-Petch limit.

For GBMP to prevail the average surface grain size must be small enough (*19*) to mitigate the generation of stacking faults (*6*). With larger grains DMP and high friction prevail. Following Yamakov et al. (*6*), grain size under stress is driven towards the dislocation splitting distance r_e, which is related to the applied stress σ_a,

$$r_e = \frac{r_0}{1 - \sigma_a / \sigma_\infty} \qquad \text{Eq. 1}$$

where r_0 is the equilibrium (zero stress) dislocation splitting distance, σ_a is an applied stress and σ_∞ is the theoretical strength of a metal(*20*), or the stress at which the splitting distance becomes infinite, $\sigma_\infty = \frac{2\gamma_{sf}}{b}$. In the following, we will use a reduced dimensionless stress parameter, $\tilde{\sigma} = \frac{\sigma_a}{\sigma_\infty}$.

Froseth et al.(*20*) define r_0 for a purely edge dislocation as,

$$r_0 = \frac{(2+\nu)Gb^2}{4\pi(1-\nu)\gamma_{sf}} \qquad \text{Eq. 2}$$

which is exclusively a function of materials properties, including Poisson’s ratio ν, stacking fault energy γ_{sf}, shear modulus G and the magnitude of the Burgers vector b, of the corresponding dislocation.

We invert the definition of equilibrium splitting distance to give the stress as a function of grain size, and choose $r_e = 2r_0$ nm, *which defines the grain size at which the onset of dislocation activity has been shown to occur* (*6*). This implies that there exists an intrinsic stability threshold for a material at $\tilde{\sigma} \sim 0.5$, corresponding to a predicted transition from GBMP to DMP that is purely defined by material properties. Above this threshold surface grain size will be driven toward a size exceeding the crossover from GBMP to DMP (i.e $d = 2r_0 \sim 17$ nm for Au). Below the threshold, grains are driven towards a size in which GBMP is maintained, leading to the often observed UNC surface layer in metals with low friction coefficients. Similarly, we can define an upper stability bound where the applied stress exceeds the theoretical strength of the material, at $\tilde{\sigma} = 1.0$. This bound indicates the onset of the stress regime in which a NC surface structure is immediately unstable.

At intermediate stresses in regime II, neglecting the stochastic resurfacing effect of wear, a transition between low and high friction will be defined by the rate of SAGG. Following Dao et al. (*10*), the shear deformation rate in FCC metals has an exponential dependence on the applied stress, σ_a, and activation volume, V^*. We use this dependence, combined with a traditional grain growth model, to form a more general expression that accounts for thermally activated grain growth, driving pressure due to GB curvature and the addition of an applied stress,

$$v_{gb} = \frac{4\gamma_{gb}}{d} M_0 \exp\left[\frac{-Q}{kT}\right] \exp\left[\frac{\left(\sigma - \frac{1}{2}\sigma_\infty\right)V^*\left(d\right)}{kT}\right] \qquad \text{Eq. 3}$$

We use this expression for grain boundary speed, v_{gb}, to describe the rate of growth in the quasi-stable regime. Here, γ_{gb} is the average grain boundary energy (J/m^2), $M_0 \exp\left[\frac{-Q}{kT}\right]$ the GB mobility (m/[s-Pa]), at surface temperature T (K), with Boltzmann's constant k. As shown below, the boundary between low and high friction in the quasi-stable regime may be calculated by using the above equation to determine the time required to grow grains to an average size $d = 2r_0$. The material property values we use to predict stability limits are defined in the supplemental [see supplemental section S3]. While a more complete model would allow activation volume to vary with grain size(*10*, *23*, *24*), this literature also suggests that for pure NC metals it is reasonable to assume an approximately constant value of $V^* \cong 10b^3$. We have compared the time calculations from both models and found only a minimal difference, so we will use the simpler model here to avoid unnecessary complication.

Determining Applied Stress and Experimental Validation of Friction Regimes Model

We calculate the maximum von Mises surface stress for a sphere-on-flat sliding contact using the Hamilton elastic contact model (*11*, *12*), which uses measured friction coefficients μ and normal force F_n values and calculated contact radius a from the Hertz elastic contact model (*11*, *12*). Hamilton's model shows that for low friction coefficients the surface stress is small, but at friction coefficients above about $\mu = 0.35$, the location of max von Mises stress shifts from the bulk to the sliding surface. It is notable that present and past data where low friction was found in unlubricated and boundary lubricated metal contacts, the friction coefficients were approximately in the range $0.1 < \mu < 0.3$, implying the maximum von Mises stress is in the bulk. In our analysis, we use Hamilton's expression for the maximum surface von Mises stress,

$$\sigma_{a,\max} = \frac{3F_n}{2\pi a^2}\left[\frac{1-2\nu}{3} + \frac{(4+\nu)}{8}\pi\mu\right] \quad \text{Eq. 4}$$

In order to test the predictions of our model, we performed experiments on self-mated Au and Cu contacts in unidirectional sliding motion with contact force that varies linearly along the length of the wear track [see supplemental section S2 for details]. Resulting friction data as a function of cycles (i.e. contact time) and maximum surface von Mises stress is then plotted using the reduced stress and time parameters,

$$\tilde{\sigma} = \frac{\sigma_{a,\max}}{\sigma_\infty} \quad \text{and} \quad \tilde{\tau} = \left(\frac{2\lambda_a}{v_s}\right)\left(\frac{4\gamma_{gb}M_0}{r_0^2}\right) \qquad \text{Eqs. 5}$$

(Fig. 1B), to demonstrate the tribological behavior regimes predicted by the model proposed in the preceding section. The reduced time parameter is effectively the ratio of time in contact of any location on the surface of a substrate to a fundamental time for grain growth. For relatively rough and evolving surfaces we do not know the effective contact length, so we chose to use the average Hertz contact diameter ($\lambda_a \sim a \sim 10\ \mu m$) as an order of magnitude estimate.

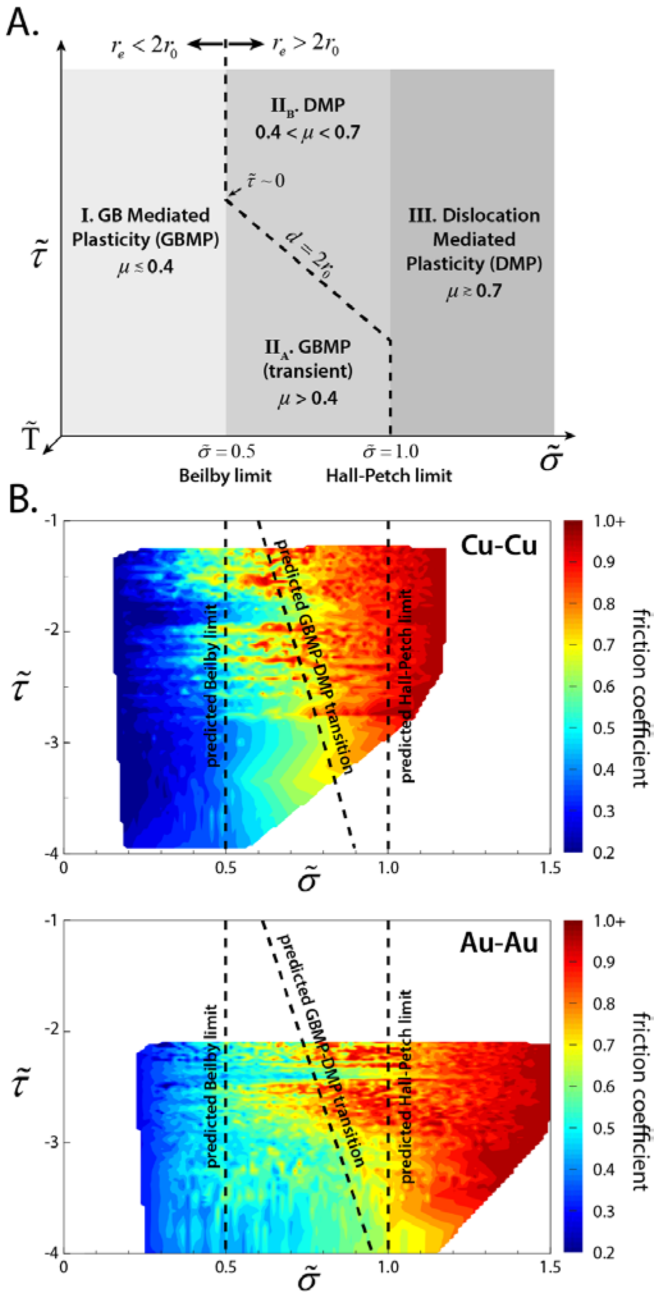

Fig. 3. *(A) Surface microstructural stability-based tribological stability regimes for metal contacts based on reduced surface stress* $\tilde{\sigma}$*, surface temperature* $\tilde{\text{T}}$*, and time* $\tilde{\tau}$ *(note that the reduced time is logarithmic, and this is a semi-log plot); and (B) phase space maps of friction behavior for Au and Cu sliding contacts with calculated predictions of regime bounds overlaid using dotted lines; in the Au-Au data there is evidence of a wear event at reduced time* $\tilde{\tau} \sim -2.5$*.*

We hypothesize that a run-in behavior will rapidly (i.e. in only a few cycles) drive surface grain size in bare or boundary lubricated metal contacts into a purely GBMP regime, $r_e \sim r_0$. The measured friction following this initially extreme deformation then follows the map shown in Fig. 3A. In all cases, the cycle proposed above dictates the tribological response: surface stress drives the grain size to the equilibrium splitting distance, r_e. The grain size dictates the active sliding mechanism, GBMP for $r_e < 2r_0$, DMP for $r_e > 2r_0$, which in turn dictates the measured friction coefficient. The friction coefficient then determines the surface stress according to the Hamilton model (*11*, *12*). Whether this cycle leads to stable, small grains (negative feedback), or unstable large grains (positive feedback) dictates the measured frictional response. We propose that this is the source of the widely characterized ultra-low wear/low friction regime for metals (*1*, *16*, *25–28*), observed for both alloys and self-mated highly pure soft metals and demonstrated here at sufficiently low contact stresses with Au-Au contacts (see wear rate Fig. S10 in supplemental). With the model presented above, we calculated predicted locations of the Beilby and Hall-Petch limits and overlay them on the friction data for both Cu-Cu and Au-Au contacts (Fig. 3), with excellent agreement. We are also able to successfully predict the boundary between low and high friction in regime II ($0.5 < \tilde{\sigma} < 1.0$) using the previous expression for GB speed to calculate the time required to coarsen average grain size from r_o to $2r_o$, as this is where the analysis by Yamakov et al. (*6*) shows that purely GBMP will transition to combined GBMP/DMP.

As shown in the simulations [see supplemental section S1], a transition to high friction with fine-grained metal contacts indicates that deformation is accommodated largely by DMP, allowing the contact surfaces to weld together at asperity contacts. This behavior is divergent, driving the system toward larger grain size, higher friction coefficient and reduced stability. Periodically it is possible to reset the process and reestablish a highly deformed, UNC layer at the surface that again drives toward high friction via coarsening. In the Au-Au friction map (Fig. 3) we see evidence of this resetting behavior, where the friction behavior along most of the wear track transitioned discontinuously back to low friction and gradually drove toward higher friction over time following the same calculated transient curve.

Evidence of the existence of a UNC layer and relatively low wear in a pure Au substrate with $\mu \sim 0.4$ at $\tilde{\sigma} \sim 0.3$ after sliding against a hard Au pin, and of a coarse grained microstructure and relatively higher wear at higher stress $\tilde{\sigma} > 0.5$ are shown in Fig. 4. In the low friction case there is evidence of a deformation band and crack formation at an angle commensurate with a tensile to compressive transition in the bulk at an angle $\theta = \arctan(\mu) \sim 18^\circ$ from the sliding plane.

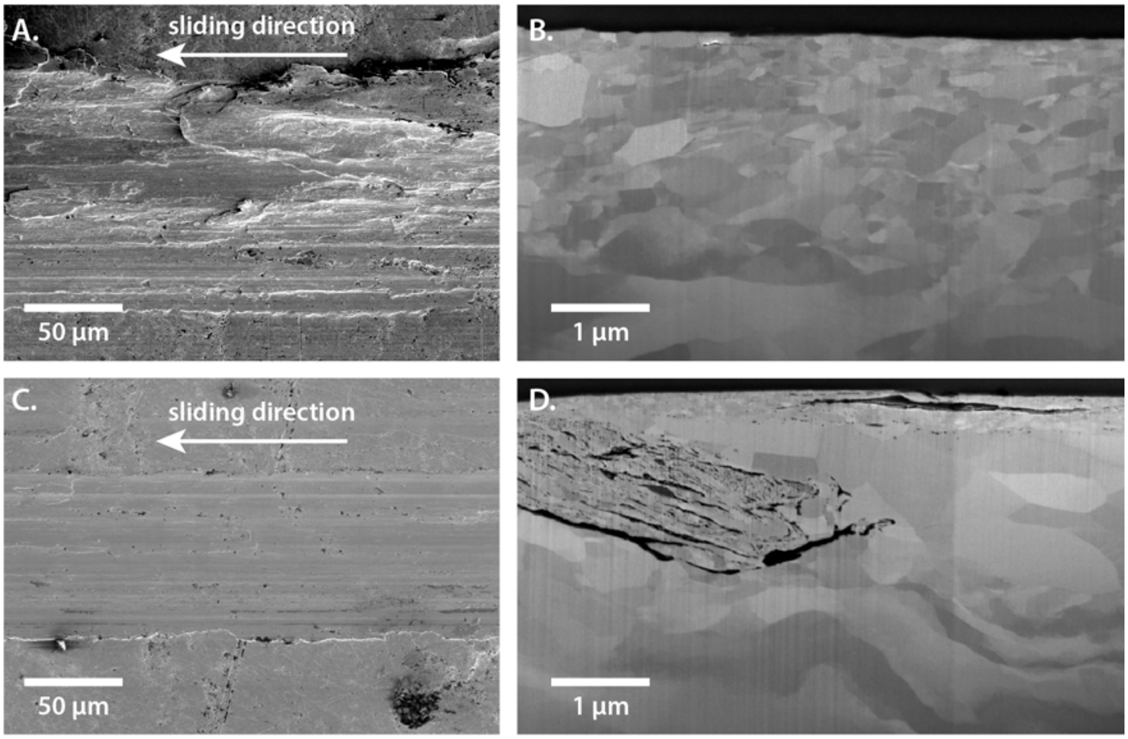

Fig. 4. *Top-down SEM images of wear tracks on a bulk pure Au substrate representative of (A) high friction (µ > 0.7) and (C) low friction (µ ~ 0.3) steady-state sliding conditions against a hard Au spherically tipped pin, and representative focused ion beam cross-section scanning electron microscope images mid-track aligned parallel to the sliding direction showing representative surface microstructures for the (B) high friction (coarse grained, d ~ 50 to 200 nm grains) and (D) low friction cases (NC, d < 50 nm grains).*

The proposed framework may be useful to determine the reduced mobility and stacking fault energy of alloys such as Ni-hardened Au, a nominally pure Au alloy (typically > 99 % Au) widely used in unlubricated sliding electrical contacts, known to have significantly improved thermal and mechanical stability, low friction and low wear. The addition of minute amounts of GB segregated Ni to Au, a system with a wide miscibility gap, primarily provides a barrier to GB mobility by pinning boundaries (*29*). The implication is that the GB mobility (M) will be reduced significantly, slowing the stress- and thermally-driven coarsening process(*30*) but not significantly impacting the GB energy or splitting distance that define the location of the nanocrystalline stability bound.

We also demonstrate that the Hall-Petch limit corresponds to the stress required to evolve surface grain structure in the span of a single contact event. This is described by Yamakov et al. (*6*) as the critical shear stress, σ_∞, where perfect dislocation slip is always favored for (111) mediated slip in FCC metals.

In some instances, for example high SFE materials that are relatively soft (e.g. pure Al), it can be shown that the Tabor limit exists below the Beilby limit, so that low friction will only be found well below a reduced stress $\tilde{\sigma} = 0.5$ [see supplemental section S3]. Friction data supporting this prediction is presented in the supplemental material (Fig. S9). Fig. S9 also shows that the significantly higher GB mobility of Al (as compared to Cu and Au, above) leads to much faster reduced times, implying near instantaneous grain growth, and that quasi-stability is not expected to exist. We expect, though, that a kinetically stabilized alloy may sufficiently slow grain growth kinetics, and make our model applicable.

The proposed model also provides an explanation for the apparent speed dependent friction behavior observed for pure and alloyed Ni by Padilla et al. (*1*) and Prasad et al. (*2*). Varying sliding speeds in the range changes the contact time per cycle, with higher speed implying slower surface evolution, and thus more cycles to affect a transition from GBMP to DMP. In the speed range of 0.1 to 10 mm/s, contact heating was shown to be negligible, removing it as a source of the speed dependence. Notable in their friction data was an apparent stress threshold below which low friction was always observed, in both cases corresponding to a Hamilton surface stress of about 500 to 600 MPa, consistent with a calculated reduced stress $\tilde{\sigma}$ = 0.5 (see supplemental section S3). Microscopy of the low friction Ni surface revealed a 50 nm thick UNC surface film with an average grain size between 5 and 10 nm (*2*). These values support the hypothesis that low friction will be associated with a surface grain size in the range $r_0 < d < 2r_0$; for Ni r_0 is calculated to be 4.9, and our model predicts that low friction would be associated with $4.9 < d < 9.8$ nm.

Summary and Conclusions

The Hall-Petch and Beilby stability limits, defining the boundaries of regimes I and III, are effectively material properties influenced primarily by SFE, a parameter that may be modified via alloying (*30, 31*). It follows that experimental determination of the bounds of regimes I and III for alloys and metal matrix composites may provide an indirect means of estimating stacking fault energy. The time-dependent behavior of materials in transient regime II, particularly the time required to transition from GBMP to DMP, also depends on materials properties. Here the behavior depends on a GB energy and mobility, where for example GB mobility can be modified by alloying to introduce kinetic stabilization mechanisms such as Zener drag (*30, 8, 7*). The proposed model provides a correlation between the time-dependent evolution in friction behavior and the rate of microstructural evolution, providing an indirect means of characterizing average mobility and GB energy, for engineered alloys.

We presented supporting evidence for the assumption that average surface grain size evolves toward a value equal to the splitting distance, $d \to r_e$. If $r_e < 2r_0$ then low friction will prevail as refinement drives surface grain size into a regime of GBMP, associated with the formation of a UNC surface film. If $r_e > 2r_0$ then the surface grains will evolve toward a regime where DMP dominates, and only metastable GBMP may be achieved via engineered nanocrystallinity and reduced GB mobility. If the reduced stress is between 0.5 and 1.0 then a transient and periodic low-to-high friction may be observed. This is a result of stress-driven grain coarsening that is reset by wear and subsequent rapid grain refinement of freshly exposed coarse grained material. For a sufficiently stable alloy, wear will occur gently but at a sufficiently high rate to prevent the surface structure from evolving into the DMP regime. This is, for example, perceived as persistent low friction in hard gold coated electrical contacts. A third (Tabor) limit exists that is a function of bulk grain size (hardness) and differs from the Hall-Petch limit that is associated with the characteristics and evolution of surface microstructure. This limit generally occurs at high reduced stresses, but for high SFE materials such as Al can exist below the Beilby limit, such that it is not possible to achieve the low friction regime at stresses up to $\tilde{\sigma} = 0.5$.

While the Hamilton model was shown to be a relatively accurate one for the calculation of applied stress, it is likely that neglected considerations may be required to make accurate predictions of material geometries sufficiently different from sphere-on-flat. For example, roughness was neglected, but this may be a stress-enhancer of sufficient magnitude to become a dominant parameter in the determination of maximum von Mises surface stress(*13*). It may also be useful to apply the transient response expression to bulk materials under stress, for example in the analysis of grain size evolution in tensile test specimens or indentation specimens after prolonged exposure to known quasi-static biaxial loads.

Acknowledgments

We thank Stephen Foiles (SNL) for enlightening discussions on determination of grain boundary and stacking fault energies via simulations and comparison with experimental values, Michael Dugger and Somuri Prasad (SNL) for numerous helpful discussions about historical research connecting tribological behavior with microstructure and surface composition, Tim Furnish for helpful comments about the stacking fault energy of alloys and Brendan Nation for assistance with design of experiments and the acquisition of friction and wear data. The authors also acknowledge helpful discussions with Jorge Argibay about time-dependent multi-variate analysis. Sandia National Laboratories is a multi-program laboratory managed and operated by Sandia Corporation, a wholly owned subsidiary of Lockheed Martin Corporation, for the U.S. Department of Energy's National Nuclear Security Administration under contract DE-AC04-94AL85000.

References

1. H. A. Padilla, B. L. Boyce, C. C. Battaile, S. V Prasad, Frictional performance and near-surface evolution of nanocrystalline Ni-Fe as governed by contact stress and sliding velocity. *Wear*. **297**, 860–871 (2013).
2. S. V. Prasad, C. C. Battaile, P. G. Kotula, Friction transitions in nanocrystalline nickel. *Scr. Mater.* **64**, 729–732 (2011).
3. N. Argibay, J. A. Bares, J. H. Keith, G. R. Bourne, W. G. Sawyer, Copper–beryllium metal fiber brushes in high current density sliding electrical contacts. *Wear*. **268**, 1230–1236 (2010).
4. L. Lu, M. L. Sui, K. Lu, Superplastic Extensibility of Nanocrystalline Copper at Room Temperature. *Science (80-.).* **287**, 1463–1466 (2000).
5. D. Wolf, V. Yamakov, S. R. Phillpot, A. Mukherjee, H. Gleiter, Deformation of nanocrystalline materials by molecular-dynamics simulation: relationship to experiments? *Acta Mater.* **53**, 1–40 (2005).
6. V. Yamakov, D. Wolf, S. R. Phillpot, a K. Mukherjee, H. Gleiter, Deformation-mechanism map for nanocrystalline metals by molecular-dynamics simulation. *Nat. Mater.* **3**, 43–47 (2004).
7. J. R. Weertman, Retaining the Nano in Nanocrystalline Alloys. *Science (80-.).* **337**, 921–922 (2012).
8. T. Chookajorn, H. A. Murdoch, C. A. Schuh, Design of Stable Nanocrystalline Alloys. *Science (80-.).* **337**, 951–954 (2012).
9. a. G. Frøseth, P. M. Derlet, H. Van Swygenhoven, Dislocations emitted from nanocrystalline grain boundaries: Nucleation and splitting distance. *Acta Mater.* **52**, 5863–5870 (2004).
10. M. Dao, L. Lu, R. J. Asaro, J. T. M. De Hosson, E. Ma, Toward a quantitative understanding of mechanical behavior of nanocrystalline metals. *Acta Mater.* **55**, 4041–4065 (2007).
11. G. M. Hamilton, Explicit Equations for the Stresses beneath a Sliding Spherical Contact. *Proc. Inst. Mech. Eng. Part C J. Mech. Eng. Sci.* **197**, 53–59 (1983).
12. G. M. Hamilton, Errata - Explicit Equations for the Stresses Beneath a Sliding Spherical Contact. *Proc. Inst. Mech. Eng. Part C J. Mech. Eng. Sci.* **197**, 282 (1983).
13. J. A. Greenwood, J. B. P. Williamson, Contact of Nominally Flat Surfaces. *Proc. R. Soc. Lond. A. Math. Phys. Sci.* **295**, 300–319 (1966).
14. J. F. Archard, Elastic Deformation and the Laws of Friction. *Proc. R. Soc. Lond. A. Math. Phys. Sci.* **243**, 190–205 (1957).

15. S. Cheng, M. Robbins, Defining Contact at the Atomic Scale. *Tribol. Lett.* **39**, 329–348 (2010).
16. N. Argibay, J. A. Bares, J. H. Keith, G. R. Bourne, W. G. Sawyer, Copper-beryllium metal fiber brushes in high current density sliding electrical contacts. *Wear*. **268**, 1230–1236 (2010).
17. N. Argibay, S V Prasad, R. S. Goeke, M. T. Dugger, J. R. Michael, Wear resistant electrically conductive Au–ZnO nanocomposite coatings synthesized by e-beam evaporation. *Wear*. **302**, 955–962 (2013).
18. K. L. Johnson, *Contact Mechanics* (Cambridge University Press, Cambridge, UK, 1985).
19. H. Van Swygenhoven, P. M. Derlet, A. G. Frøseth, Stacking fault energies and slip in nanocrystalline metals. *Nat. Mater.* **3**, 399–403 (2004).
20. A. G. Frøseth, P. M. Derlet, H. Van Swygenhoven, Dislocations emitted from nanocrystalline grain boundaries: Nucleation and splitting distance. *Acta Mater.* **52**, 5863–5870 (2004).
21. H. Van Swygenhoven, P. Derlet, A. Hasnaoui, Atomic mechanism for dislocation emission from nanosized grain boundaries. *Phys. Rev. B*. **66**, 024101 (2002).
22. G. I. Finch, a. G. Quarrell, J. S. Roebuck, The Beilby Layer. *Proc. R. Soc. A Math. Phys. Eng. Sci.* **145**, 676–681 (1934).
23. J. R. Trelewicz, C. A. Schuh, The Hall–Petch breakdown in nanocrystalline metals: A crossover to glass-like deformation. *Acta Mater.* **55**, 5948–5958 (2007).
24. R. J. Asaro, S. Suresh, Mechanistic models for the activation volume and rate sensitivity in metals with nanocrystalline grains and nano-scale twins. *Acta Mater.* **53**, 3369–3382 (2005).
25. D. Kuhlmann-Wilsdorf, in *Electrical Contacts Principles and Applications*, P. G. Slade, Ed. (Marcel Dekker, New York, 1999), pp. 943–1017.
26. N. Argibay, W. G. Sawyer, Low wear metal sliding electrical contacts at high current density. *Wear*. **274–275**, 229–237 (2012).
27. J. L. Johnson, J. Schreurs, High-Current Brushes, Part VIII: Effect of Electrical Load. *Wear*. **78**, 219–232 (1982).
28. S V Prasad, J. R. Michael, T. R. Christenson, EBSD studies on wear-induced subsurface regions in LIGA nickel. *Scr. Mater.* **48**, 255–260 (2003).
29. C. C. Lo, J. A. Augis, M. R. Pinnel, Hardening mechanisms of hard gold. *J. Appl. Phys.* **50**, 6887–6891 (1979).
30. N. Argibay *et al.*, On the thermal stability of physical vapor deposited oxide-hardened nanocrystalline gold thin films. *J. Appl. Phys.* **117**, 1–13 (2015).
31. F. Huang, N. R. Tao, Effects of Strain Rate and Deformation Temperature on Microstructures and Hardness in Plastically Deformed Pure Aluminum. *J. Mater. Sci. Technol.* **27**, 1–7 (2011).
32. I. L. Dillamore, R. E. Smallman, W. T. Roberts, A determination of the stacking-fault energy of some pure F.C.C. metals. *Philos. Mag.* **9**, 517–526 (1964).
33. F. J. Humphreys, M. Hatherly, Eds., *Recrystallization and Related Annealing Phenomena* (Elsevier, Oxford, UK, ed. 2nd, 2004).
34. J. F. Archard, Contact and Rubbing of Flat Surfaces. *J. Appl. Phys.* **24** (1953).

Supplemental Material

S1. Simulation Methods and Additional Results/Analysis

[Attached separately, "Modeling Supplemental"]

S2. Experimental Methods, Materials and Characterization

The Au-Au contact consisted of a 1.59 mm radius spherically-tipped bulk hard gold alloy pin (Deringer-Ney Inc., Neyoro-G alloy) brought into sliding contact with a high purity (> 99.999 %) bulk gold ingot. Details of the pin composition and preparation are described elsewhere(*17*). The pure Au ingot was not polished to avoid transfer and embedding of hard particle media, instead it was pressed between polished WC plates (average roughness, R_a < 20 nm) in a hydraulic press to 3 ksi pressure to achieve a smooth surface finish, yielding an average roughness R_a ~ 375 nm measured using a scanning white light interferometer (SWLI; Bruker Contour GT). The Cu-Cu contact consisted of a 1.19 mm radius UNS C10100 Cu ball bearing (McMaster-Carr) and a high purity (> 99.999 %) bulk single crystal substrate (Princeton Scientific, Princeton, NJ) with average surface roughness < 10 nm and an initial surface orientation of <100>. The hard Au substrate used to acquire the wear and friction data in Fig. S10 consisted of the same type of hard gold alloy pin sliding against a 2 um thick electroplated type I Ni-hardened gold film (Theta Plate, Albuquerque, NM) on an 50/50 wt % Fe/Ni substrate. For the case of Cu-Cu an inert gas (ultra-high purity N_2) was used to shield the contact and prevent oxidation.

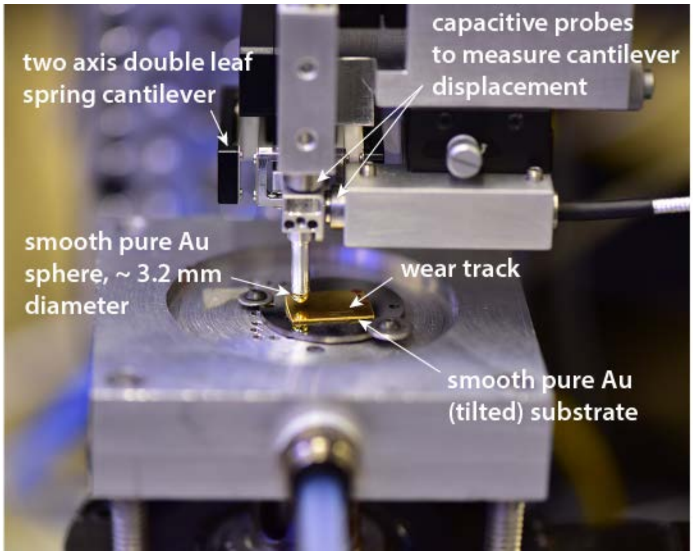

Fig. S7. *Annotated photograph of tribometer showing a sliding experiment between a smooth pure Au ball and a pure Au substrate.*

The instrument used for friction measurements is shown in Fig. S7 and functionally the same as the instrument described in a previous publication(*26*). A brief summary of the instrument is given here. Orthogonal capacitance probes measured the deflection of a double-leaf spring cantilever (Anton Paar Standard and High Load cantilevers were used). Data was acquired at 100 Hz throughout sliding. Positioning stages Sample preparation is described in detail elsewhere(*17*), generally consisting of turning spherical tips on the Au alloy pins using a lathe, polishing and rinsing with acetone then isopropyl alcohol prior to each experiment. The same rinse was used for all surfaces, though the Cu balls were dipped in an oxide reducing agent (bright dip) prior to testing. Fresh Au pins and Cu balls were used for each experiment. Flat substrates were fixtured with a small prescribed tilt designed to achieve a linear contact force ramp from 0 to 100 mN over a 10 mm long wear track. Sliding was unidirectional, with contact force linearly increasing during a cycle, at a constant 1 mm/s sliding speed. A pin or sphere was brought out of contact before returning to the starting position for the next cycle, also at 1 mm/s. For the data shown in Figs. 1 and 3 a total of 100 sliding cycles were used.

Characterization of the near-surface microstructure was done with a dual-beam FEI Helios Nanolab scanning electron microscope-focused ion beam (SEM-FIB). A trench was milled in the middle of wear tracks where high or low friction were measured, with the cross-sectioned plane oriented parallel to the sliding direction, and imaged using a secondary electron (SE), through-the-lens detector at 5 kV to produce the images shown in Fig. 4 B and D. Top-down imaging was performed with an Everhart-Thornley SE detector also at 5 kV to produce images shown in Fig. 4 A and C.

S3. Generation of friction stability maps and soft and evidence of the Tabor limit

The material parameter values used to calculate splitting distance, Hamilton contact stresses and reduced stresses are provided in Table S1.

Table S1. Material properties and calculated parameters(*32*, *33*).

property	**material system**				
	Au	*Cu*	*Al*	*Ni*	*units*
shear modulus, *G*	27	48	27	76	GPa
Poisson ratio, *v*	0.44	0.36	0.35	0.31	-
lattice constant, *a*	4.08	3.61	4.05	3.52	Å
Burgers vector, *b*	2.88	2.55	2.86	2.49	Å
SFE, γ_{sf}	45	78	166	128	mJ/m^2
GBE, γ_{gb}	378	625	324	-	mJ/m^2
HAGB mobility, M_0	3.84 x 10^{-6}	30	2 x 10^{-2}	-	m/s-Pa
activation energy, *Q*	1.33	2.01	1.05	-	x10^{-19} J
calculated parameters					
splitting distance, r_0	8.7	5.9	2.0	4.9	nm
σ_∞	312	611	1,117	1,029	MPa
$\sigma_a\left(r=2r_0\right)$	156	306	559	514	MPa

A stepwise progression of the analysis used to generate the general friction behavior maps shown in Fig. 3 is presented in Fig. S8.

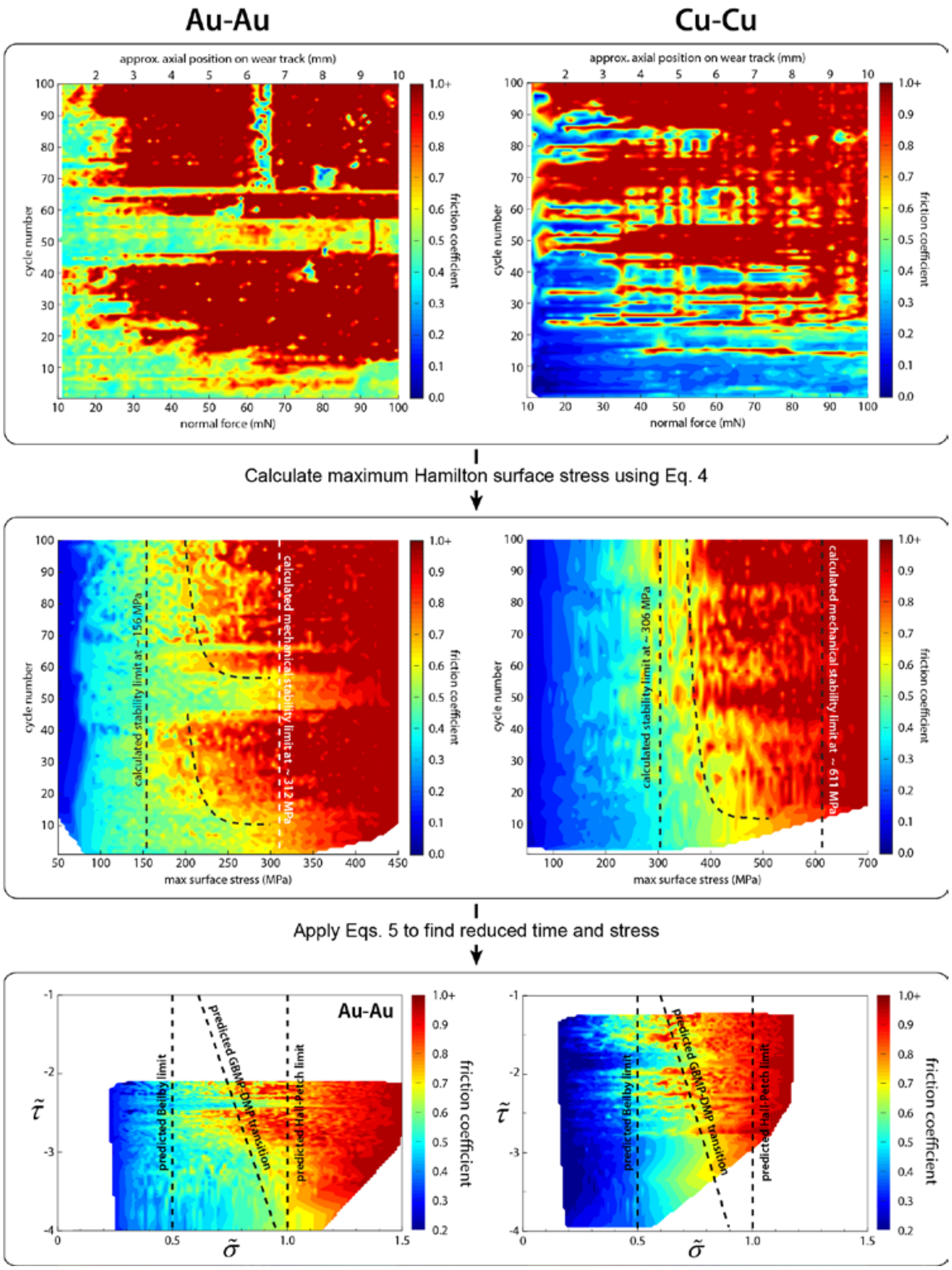

Fig. S8. Plots showing stepwise progression from raw data to the generation of maps shown in Fig. 3.

Friction maps were also produced for high purity (> 99.999 %) aluminum (Fisher Scientific, initial R_a ~ 600 nm) sliding against a sphere of 1100 Al over the normal force range 0 to 100 mN for 100 cycles. An inert cover gas (ultra-high purity N_2) was used to prevent oxidation here as well. Data for Al is shown in Fig. S9. As discussed in the main text, this data reveals a different behavior, evidence of the existence of the Tabor limit, as it was predicted to be found well below the Beilby limit for Al due to relatively high SFE (Table S1) and low hardness. Due to grain size evolution as a result of deformation induced by sliding we can only estimate hardness by conservatively estimating bulk grain size. The Tabor limit was predicted to exist well below the Beilby limit, at reduced stress near 0.1 or 0.2. The data reveals that the transition from low to high friction did in fact occur at about this reduced stress, well below 0.5. While the bulk grain size near the surface of the pure Al substrate would have evolved rapidly, the bulk grain size is expected to be coarse. As a first order estimate, yield strength values were taken from literature from experimental micro hardness tests, and for a conservative range of average grain size between 100 to 500 nm the hardness should be about 350 to 700 MPa(*31*), implying that the Tabor limit should be found somewhere in the reduced stress range $0.1 < \tilde{\sigma} < 0.2$, in agreement with data.

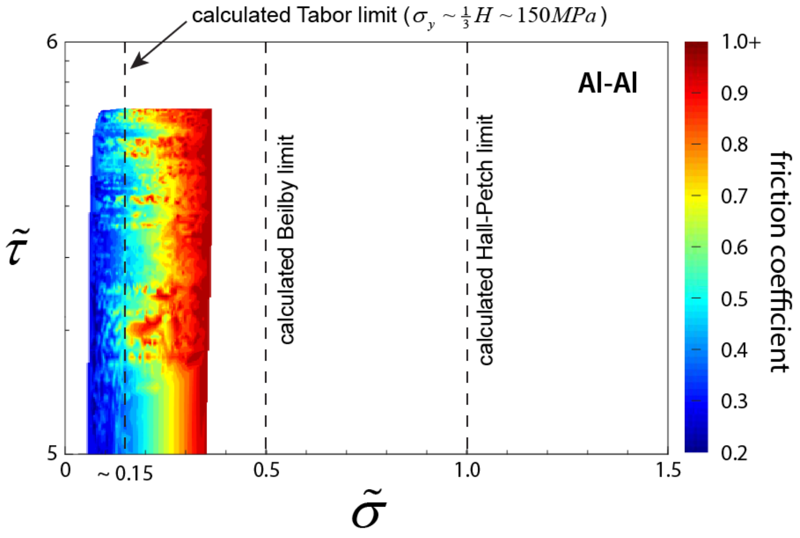

Fig. S9. *Friction map for high purity (> 99.999 %) Al flat sliding against an 1100 Al sphere. This data supports the hypothesis that for soft, high SFE materials the Tabor limit will be smaller than the Beilby limit and transition from low to high friction will occur at relatively small max surface stresses.*

S4. Unlubricated and boundary lubricated metal-on-metal wear and friction behaviors are correlated, but not in a predictable way

Measurements of wear as a function of contact stress were carried out on flat substrates of pure and hard Au, corresponding in the case of pure Au to the friction data shown in the manuscript. A scanning white light interferometer (SWLI; Bruker Contour GT) was used to measure average cross-sectional area of the wear track in 1 mm intervals along the wear track length. Each image was approximately 310 um x 230 um, with a vertical (depth) resolution of about 10 nm. Due to the fact that contact force was ramped linearly for these experiments the force varied by about 3 % of the maximum value of the linear ramp in the track length span of each image. The average value of contact force in the span of each image was used for the calculation of specific wear rate (mm^3/N-m), using the following expression. Here, F_n is the contact force, N is the cycle number and A is the average cross-section of the wear track, only including material missing below the reference plane outside the wear track.

$$K = \frac{\left(1000\,\frac{mm}{m}\right)A}{F_n \cdot N} \qquad (\text{mm}^3/\text{N-m})$$

As shown in Fig. S10 for a pure Au and for a type I Ni-hardened Au substrate after 100 cycles of sliding against the same spherically-tipped hard Au alloy pins described earlier, while wear rate was proportional to normal force (or maximum Hertz stress), friction behavior was not. Instead, the success of utilizing Hamilton's model and the maximum surface von Mises stress as a metric for the transition between deformation mechanisms, associated with low (GBMP) or high (DMP) friction, implies that friction regimes are not directly predictive of wear rate. This data challenges the longstanding assumption that high hardness results in low friction and wear in metal contacts (*34*), revealing the need for a more profound understanding and consideration of material properties and microstructural evolution in the process of predicting the ability to achieve low wear and friction with metals in contact, and not merely a consideration of derivative parameters such as hardness.

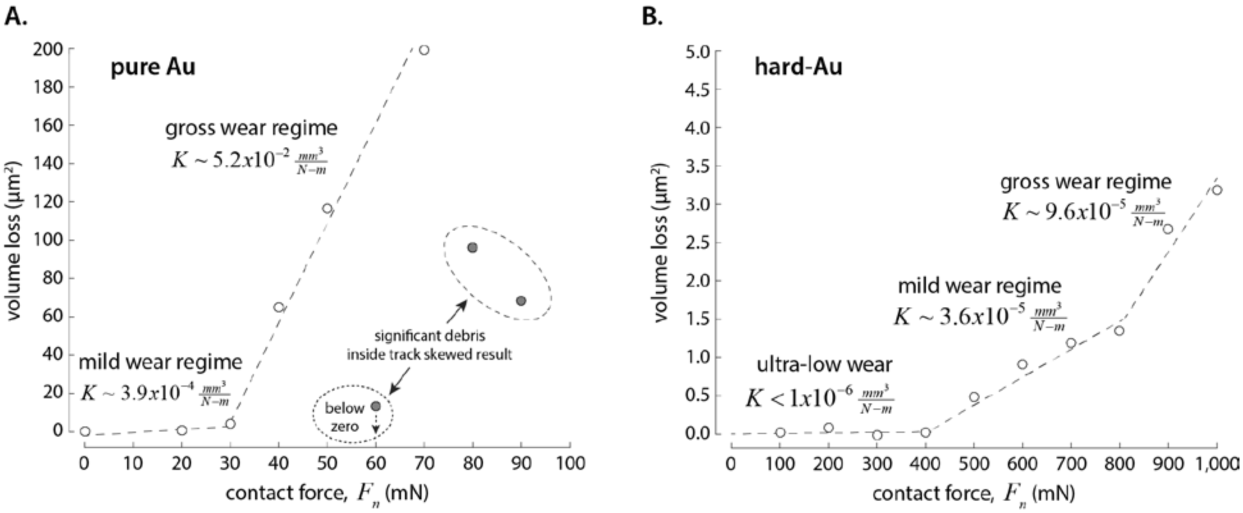

Fig. S10. *Wear data for (A) pure and (B) hard (type I ASTM Ni-hardened) gold substrates after sliding against spherically-tipped hard Au pin (Neyoro G, Derringer-Ney Corp.) in ramped force experiments. Note that y-axis and x-axis ranges differ; wear volumes measured using a scanning white light interferometer (Bruker Contour GT).*

S1. Simulation Methods and Additional Results/Analysis

Our atomistic simulations use the embedded atom method (EAM), with the alloy potential for the Ag/Cu mixtures from Wu and Trinkle.[1] Although the experimental phase diagram shows that Ag and Cu are nearly immiscible at room temperature, this EAM potential has been optimized for surface diffusion of Cu islands on Ag, predicting mixing of the bulk materials and is therefore suitable for our purposes here. We have chosen to model Ag contacts, instead of Au, because of this available and proven EAM potential. We expect that, while results from simulations of Ag are interesting in their own right, they are also applicable to Au. This is primarily due to the similarities in the mechanical properties of the two materials. Ag and Au are both noble metals with low stacking-fault energies, and have very similar bulk and shear moduli, hardness and Poisson's ratios. We have also performed simulations on pure Au contacts and the results are nearly identical to those presented here for pure Ag. For the reported simulations we created a nanocrystalline Ag substrate by melting a bulk FCC crystal of Ag at 1800 K and rapidly quenching it to 300 K over 100 ps. The resulting structure is intended to model a tribological surface after run-in, with grains of approximately 5 nm in diameter and a strong {111} surface texture. Part of a 2-dimensional slice through the center of this 3-dimensional microstructure is shown in Fig. S1(a), where atoms locally in an FCC environment are colored according to their grain membership, those locally in an HCP environment (i.e., twins and stacking faults) are colored red, and those that cannot be classified as either FCC or HCP (i.e. grain boundaries) are colored black. The preferential alignment of twins and stacking faults parallel to the free surfaces at the top and bottom of the substrates indicate that the surface texture being dominated by {111} planes. Also shown in Fig. S1(a) is the tip we use to model a single asperity contact. This tip is a spherical cap with a 10 nm radius of curvature and is copied from the interior of the nanocrystalline slab used as the substrate. This practice ensures that the tip has an initial microstructure differing from the substrate surface, as shown in Fig. S1(a).

Our MD simulations were performed with LAMMPS using a velocity-Verlet integration scheme with a timestep of 1 fs. The tip is brought into contact with the substrate by moving a rigid thin layer at the top of the tip, which will be called the loading layer, downward at a fixed velocity of 0.2 m/s. Shear is imposed by moving the loading layer laterally at a velocity of

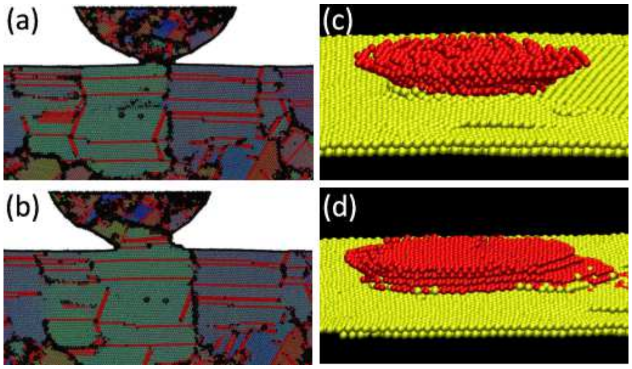

Figure S1: Grain analysis of tip-slab contact (a) before sliding and (b) after 6nm of sliding. (c) and (d) are snapshots of atoms as in (a) and (b), respectively, but only showing the bottom of the tip (red) and the top of the substrate (yellow).

2 m/s. Another thin layer of atoms at the bottom surface of the substrate is also held rigid to allow for the control of compression and sliding. A layer of atoms adjacent to the bottom rigid layer in the substrate is used to control the temperature of the system at 300 K via a Langevin thermostat applied only in the direction orthogonal to compression and shear. We have calculated the temperature at the sliding interface and found only a minimal rise ($\sim$10 K). The substrate is 67 nm long in the shear direction, 34 nm high, and 17 nm deep (i.e., in the direction orthogonal to compression and shear).

When the tip approaches and contacts the substrate surface, we find cold welding of the tip and the substrate, with an adhesive strength $\sim$ 4GPa,[2] in reasonable agreement with experimental measurements,[3, 4]. With further compression the attractive regime is followed by a repulsive force as the tip becomes more heavily deformed and embedded in the substrate. We chose a number of different separations between the tip and substrate at which shear simulations were performed. In all cases, we find that, after cold-welding, the tip undergoes microstructural reorientation to form a single grain across the interface,[5] as shown in Figs. S1 (a) and (b). This reorientation typically occurs during the first 4nm of sliding; a distance that is only slightly larger than the width of the initial contact. Figures S1 (c) and (d) show rendered snapshots including only atoms at the very bottom of the tip and the top of the substrate, which are colored red and yellow, respectively. The microstructural reorganization after shear is clear.

Figure S1 demonstrates that the contact has become commensurate dur-

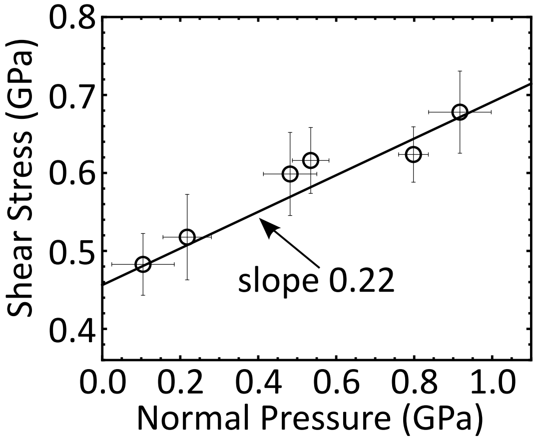

Figure S2: Shear stress vs. normal pressure for an Ag spherical tip sliding over an Ag flat substrate.

ing sliding, and that sliding occurs at the FCC slip planes, which in this case are along $\{111\}$ planes and in the $\langle 110 \rangle$ direction. The commensurate contact leads to a saw-tooth signal in the friction trace, indicating the atomic-scale stick-slip behavior that has been experimentally observed previously.[6] It has been understood that the sliding between two commensurate surfaces yields high friction,[7] and in this case results in a friction coefficient $\mu = 0.22$, as calculated from the slope of the shear stress vs. normal pressure curve (see Fig. S2). This coefficient compares very well with our experimental results on gold ($\mu = 0.20$). The comparison between experiments and simulations is shown later in Fig. S5 where results on alloys are also included.

To study the effects of alloying we randomly replaced 12.5% of Ag atoms in the previous system with Cu atoms to arrive at the composition of sterling silver. While Cu is soluble to only 1% in Ag at room temperature,[8] both the specifics of the EAM potential as well as the timescales accessible to our simulations obviate the segregation of the alloy into Ag-rich and Cu-rich phases. However, for the tip-slab contact geometry, we find that the calculated work of adhesion in the alloy is almost twice that of the pure metal. This higher adhesion in the Ag/Cu alloy makes tip simulations infeasible because all simulations, regardless of initial starting load, lead to steady state sliding with the same values of loading and friction forces. To circumvent this difficulty we shift to a contact between two Ag/Cu slabs created by duplicating and translating the bulk substrate. A snapshot of this sliding geometry is shown in Fig. S3 with white dots indicating the location of the sliding interface. This plane has been identified by examining the velocity profile along the vertical (z) direction, which indicates that the majority of sliding occurs at the middle of the system (i.e., the contact between two slabs). The added advantage of this geometry is that both pure Ag and Ag/Cu alloys exhibit nearly identical adhesion in force vs. separation curves.

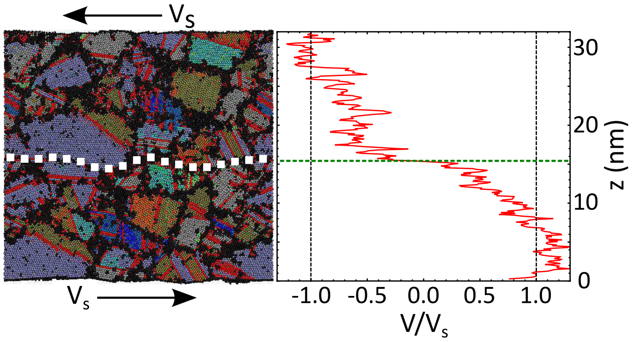

Figure S3: Snapshot of a simulation of contact between two Ag/Cu slabs (left). The sliding primarily occurs at the interface of the two slabs, as is shown in the velocity profiles (right). Here V_s is the velocity of the rigid loading layer.

To enable more direct comparisons between the pure metal and the alloy, we also simulated a slab-slab contact for pure Ag. Figure S4(a) shows the calculated shear stress for such a contact, which exhibits a nontrivial profile with three distinct regimes. The underlying reason is that the nanocrystalline Ag slabs undergo significant grain coalescence and growth under shear and the sliding plane moves toward the rigid loading layer as the shear proceeds. Detailed grain analysis indicates that in regime I the sliding is primarily accommodated through the slip plane at the middle of the system (i.e., close to the initial interface between the two slabs). However in regime II the sliding plane gradually moves towards one surface of the system during shear because of the grain growth across the initial contacting interface (similar to Fig. S1(b)). In regime III sliding primarily occurs at the interface between the elastic domain and the rigid loading layer used to impose the shear. Here by "elastic" we mean that atomic interactions are calculated via EAM potentials as described earlier and have no constraints imposed on their motion such as those used to produce a rigid layer. Because grain growth is stopped by the rigid layer, the interface is essentially a

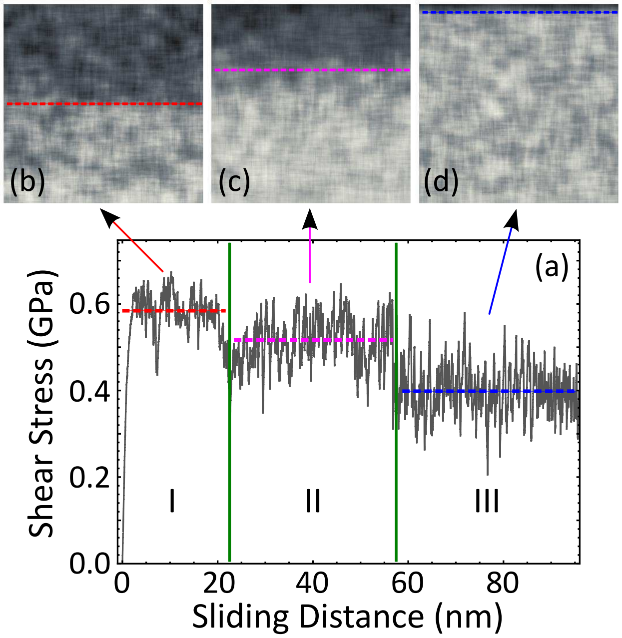

Figure S4: Contact between two Ag slabs under shear: (a) Friction trace as a function of sliding distance showing three distinct regimes: I and (b), high friction and sliding primarily occurs via slip planes near the initial interface between the two slabs; II and (c), intermediate friction and sliding plane moves towards the loading layer; III and (d), low friction and sliding primarily occurs at the boundary of the loading layer. (b)-(d) are gray-scale density plots of the local shear velocity.

grain boundary traversing the system at the contact between a transfer film (that grows at the rigid loading layer) and the bulk, elastic polycrystal. As a consequence of the movement of the sliding plane and the change of sliding mechanism, the friction exhibits the transition(s) shown in Fig. S4(a).

For Ag/Cu alloys, grain coalescence and growth are not observed and the sliding always occurs near the initial contact between the two slabs (Fig. S3). The friction for the alloy does not show the transition behavior as in Fig. S4(a) but instead stays almost constant after the initial run-in period. Since for pure Ag only in regime I the sliding occurs near the initial slab-slab interface, we will take the mean friction in this regime and compare with that of Ag/Cu systems. The results are shown in Fig. S5(a), with friction coefficient $\mu = 0.027$ for the alloy and $\mu = 0.076$ for the pure metal. To compare with the experimental results (on gold) obtained with a slider-plate contact, we use a scaling factor of 3 for μ to account for the geometrical differences between the slab-slab to the tip-slab geometry. This factor has been reported in previous work from our group [9] and from Knippenberg *et al.*[10], and is consistent with the results reported here on pure Ag ($\mu = 0.076$ vs. $\mu = 0.22$ for the slab-slab and tip-slab geometries, respectively). Using this factor, we arrive at a friction coefficient of 0.081 for the alloy tip-slab contact with 87.5% Ag and 12.5% Cu in terms of number of atoms. The results on μ from experiments (on pure Au and Au/Cu alloys) and simulations (on pure Ag and on Ag/Cu alloys) are summarized in Fig. S5(b), and the two are in close agreement with each other.

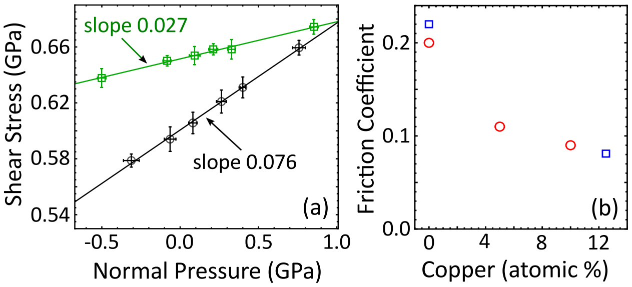

Figure S5: (a) Friction vs. load for the slab-slab contact of pure Ag (circles) and Ag/Cu alloy (squares); (b) Friction coefficient vs. the atomic percentage of Cu in Ag matrix: experiments (circles) vs. simulations (squares). Note that the experimental results are for pure Au and an Au/Cu alloy.

We now discuss the atomic-scale mechanism behind the lower friction coefficient in alloys. In the Ag/Cu alloy, rather than a commensurate contact forming, grains remain predominantly distinct across the cold-welded slabs, and sliding is found to proceed along the new grain boundaries formed at the junction. This is in contrast to pure Ag slabs, which undergo grain growth to the point where effectively a bulk polycrystal is sheared against the loading layer rather than distinct slabs sliding against each other. Only in the initial stage (regime I in Fig. S4) does the sliding occur via stacking faults (i.e., along the FCC slip planes). We propose that dislocation-mediated processes are responsible for the high friction coefficient in pure Ag as observed with the tip-slab contact and the slab-slab contact in the earlier sliding stage. In alloys the suppression of grain reorientation and growth, likely because of the mismatch in lattice constant, suppresses this sliding mechanism, and instead leads to grain-boundary mediated sliding with a lower friction coefficient.

To demonstrate the validity of this hypothesis, we further studied a geometry that allows the same contact geometry for both materials while forcing the sliding mechanism to be identical. We then would expect similar friction coefficients in both cases. To investigate this, we use a rigid plate of nanocrystalline Ag (or Ag/Cu) sliding against a thick elastic Ag (or AgCu) substrate. Since rigid atoms in the plate suppress the grain coalescence and growth, sliding occurs along grain boundaries in both the pure metal and the alloy. This case is discussed in detail below. Another option for suppressing the grain reorientation is to use rigid tips of a spherical-cap shape, modeling single asperity experiments in which the tip material is much harder than the substrate. We have performed these simulations as well and found the calculated μ in both cases to be near 1.0. Such high friction coefficients are due to the fact that the rigid tip leads to substantial plowing of and damage to the substrate material. A further motivation for the rigid plate geometry is to avoid this plowing deformation.

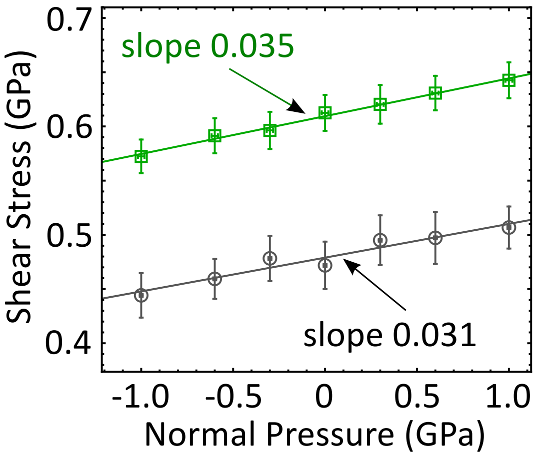

Figure S6: Friction vs. load for a rigid plate sliding over an elastic slab: pure Ag (circles) and Ag/Cu alloy (squares)

The grain analysis and velocity profiles (not shown) demonstrate that for both the pure Ag and the Ag/Cu alloy, cold welding of the rigid plate to the substrate occurs, and a ~ 1 nm thick transfer film forms at the contact. Moving the rigid plate laterally at a constant velocity of 2 m/s leads to sliding predominantly along the boundary between the transfer film and the substrate. This boundary itself consists of multiple linked grain boundaries where grains in the transfer film end and those in the substrate begin. As hypothesized, the rigid plate suppressed the grain coalescence even for pure Ag and the sliding occurs along grain boundaries in both systems. The friction of the two systems is compared in Fig. S6, with $\mu = 0.031$ for the pure Ag and $\mu = 0.035$ for the Ag/Cu alloy. Note that the friction coefficient is even slightly larger for the alloy in the rigid plate geometry. This is in sharp contrast with the results in Figs. S2 and S5, where, for the same contact geometry (a tip sliding over a slab), different sliding mechanisms in the pure Ag and the Ag/Cu alloy make the friction coefficient of the former larger by a factor of 3.

Figure S6 also demonstrates the effect of the materials properties on the friction. Experimentally it is difficult to determine the true contact area, and thus an effective shear strength of contacts is generally calculated, as opposed to the true interfacial shear strength. Here we have the benefit of knowing the contact area precisely and can compare the interfacial shear strength of the two materials, by comparing the calculated shear stress at zero applied pressure. We find interfacial shear stresses of 513 MPa for the pure Ag and 653 MPa for the Ag/Cu alloy, indicating that the hardness of the materials leads at best to a slight increase in the friction force for the alloy and cannot be responsible for the reduction in μ compared to pure metals. We note that while the hardness should not have a strong contribution to friction measurements with an infinite rigid plate, both the alloy and the pure metal have the same initial grain size, indicating that the hardness is likely comparable. The calculated ratio of interfacial shear stress of the pure Ag and the Ag/Cu alloy from the rigid-tip simulations (i.e., with a plowing mechanism) is nearly identical to the ratio in Fig. S6.

References

[1] Henry H. Wu and Dallas R. Trinkle. Cu/Ag EAM potential optimized for heteroepitaxial diffusion from ab initio data. *Comp. Mater. Sci.*, 47:577–583, 2009.

[2] B. Bhushan, J. N. Israelachivili, and U. Landman. Nanotribology - friction, wear and lubrication at the atomic-scale. *Nature*, 374:607–616, 1995.

[3] R. C. Thomas, J. E. Houston, T. A. Michalske, and R. M. Crooks. The mechanical response of gold substrates passivated by self-assembling monolayer films. *Science*, 259:1883–1885, 1993.

[4] N. A. Alcantar, C. Park, J.-M. Pan, and J. N. Israelachvili. Adhesion and coalescence of ductile metal surfaces and nanoparticles. *Acta Mater.*, 51:31–47, 2003.

[5] Y. Lu, J. Y. Huang, C. Wang, S. Sun, and J. Lou. Cold welding of ultrathin gold nanowires. *Nature Nanotech.*, 5:218–224, 2010.

[6] Nitya Nand Gosvami, Michael Feldmann, Joël Peguiron, Michael Moseler, André Schirmeisen, and Roland Bennewitz. Ageing of a microscopic sliding gold contact at low temperatures. *Phys. Rev. Lett.*, 107:144303, 2011.

[7] G. He, M. H. Muser, and M. O. Robbins. Adsorbed layers and the origin of static friction. *Science*, 284:1650–1652, 1999.

[8] T. Lyman, editor. *Metals Handbook (Volume 8): Mettalography, Structures and Phase Diagrams.* American Society for Metals, Materials Park, 1973.

[9] M. Chandross, C. D. Lorenz, M. J. Stevens, and G. S. Grest. Simulations of nanotribology with realistic probe tip models. *Langmuir*, 24:1240–1246, 2008.

[10] M. T. Knippenberg, P. T. Mikulski, and J. A. Harrison. Effects of tip geometry on interfacial contact forces. *Model. Simul. Mater. Sci. Eng.*, 18:034002, 2010.